Energy Fuels **2011,** *25,* 835–842 · DOI:10.1021/ef101548g
Published on Web 01/20/2011

energy&fuels
article

Adsorption Equilibrium and Kinetics of CO_2 on Chromium Terephthalate MIL-101

Zhijuan Zhang, Sisi Huang, Shikai Xian, Hongxia Xi, and Zhong Li*

School of Chemistry and Chemical Engineering, South China University of Technology, Guangzhou 510640, China

Received August 15, 2010. Revised Manuscript Received December 26, 2010

In this work, isotherm and kinetics of CO_2 adsorption on a chromium-based metal organic framework MIL-101 sample were studied. The MIL-101 crystal cubes were synthesized by the microwave irradiation method and then characterized. The isotherms and kinetic curves of CO_2 adsorption on the MIL-101 sample were separately measured at 298, 308, 318, and 328 K within a pressure range of 0−30 bar by a gravimetric method. The mass-transfer constants and diffusion activation energy E_a of CO_2 adsorption on the MIL-101 crystals were estimated separately. Results showed that the maximum uptake of CO_2 on MIL-101 was 22.9 mmol/g at 298 K and 30 bar and that isotherms of CO_2 adsorption were well-fitted with the Freundlich model. The isosteric adsorption heat of CO_2 on MIL-101 was in the range of 4.0−28.6 kJ/mol. It depended upon the amount of CO_2 uptake and decreased with the loading of CO_2. The adsorption kinetics of CO_2 on the MIL-101 crystals was described by the linear driving force (LDF) model. With the increase of the temperature, the mass-transfer constants of CO_2 adsorption on MIL-101 increased. The diffusion coefficients of CO_2 were in the range from 4.11×10^{-11} to 2.54×10^{-10} cm^2/s. The coefficients increased with the temperature and decreased with the pressure. The diffusion activation energies E_a of CO_2 on MIL-101 were in the range of 2.62−4.24 kJ/mol, which decreased with the pressure.

1. Introduction

Fossil fuels supply more than 85% of the world's energy needs. However, the use of fossil fuels is coupled to the increasing emission of a large amount of greenhouse gas carbon dioxide (CO_2). The ambient concentration of CO_2 is projected to increase from about 280 ppm from the pre-industrial revolution period (early 1900s) to 450 ppm by 2050 if no action is taken to mitigate greenhouse gas emissions.[1] Improving the efficiency of energy use and increasing the use of low-carbon energy sources are considered to be potential ways to reduce CO_2 emissions.[2] In addition, there is growing recognition that capturing and permanently sequestering CO_2 must be part of the solution to curb greenhouse gas emissions. In recent years, the development of suitable CO_2 capture and sequestration technologies has become a key issue to be addressed by the scientific community. Research in this field mainly concerns several CO_2 capture technologies or methods, such as amine-based absorption, membrane-based separation, adsorption, and cryogenic separation.[3] The capture of CO_2 by adsorption has been identified as one potential solution to reduce greenhouse gas emissions. The success of this approach is mainly dependent upon the development of a low-cost adsorbent with a high CO_2 selectivity and adsorption capacity. The adsorption of CO_2 on conventional zeolites,[4−7] activated carbons,[8−10] and coals[11] had been investigated by many researchers. Because the adsorption performance of these conventional adsorbents for CO_2 could not meet the requirement of their commercial application, future applications of adsorption are still limited by the availability of new and better adsorbents. Recently, many research activities were focused on the development of novel adsorbents, such as modified activated carbons and modified zeolites, by means of surface modification for enhancing CO_2 adsorption or the development of metal−organic frameworks (MOFs) for CO_2 adsorption. Zhao et al.[12] synthesized a $AlPO_4$-14 molecular sieve and reported that the CO_2 adsorption capacity of $AlPO_4$-14 was up to 2.0 mmol/g at 300 K. Zhang et al.[13] modified activated carbon with a high surface area using ammonia impregnation, then studied its adsorption isotherms of CO_2, and found that the modified activated carbon had a higher CO_2 adsorption capacity compared to the original activated carbon, which was more than 3.0 mmol/g at 1.0 bar and 298 K. Currently, MOFs are rapidly developed as promising alternative adsorbents for CO_2 capture because of their extra-high porosity, regular porous structures, with pore sizes and chemical functionalities

*To whom correspondence should be addressed. Fax: +86-20-87110608. E-mail: cezhli@scut.edu.cn.

(1) Liang, Z. J.; Marshall, M.; Chaffee, A. L. *Energy Fuels* **2009**, *23*, 2785–2789.
(2) Díaz, E.; Muñoz, E.; Vega, A.; Ordóñez, S. *Chemosphere* **2008**, *70*, 1375–1382.
(3) Gupta, M.; Coyle, I.; Thambimuthu, K. Strawman document for CO_2 capture and storage (CC&S) technology roadmap. *Proceedings of the 1st CC&S Technology Roadmap Workshop*; Calgary, Alberta, Canada, Sept 18 and 19, 2003.
(4) Siriwardane, R. V.; Shen, M. S.; Fisher, E. P.; Poston, J. A. *Energy Fuels* **2005**, *19*, 1153–1159.
(5) Su, F. S.; Lu, C. S.; Kuo, S. C.; Zeng, W. T. *Energy Fuels* **2010**, *24*, 1441–1448.
(6) Siriwardane, R. V.; Shen, M. S.; Fisher, E. P. *Energy Fuels* **2003**, *17*, 571–576.
(7) Jadhav, P. D.; Chatti, R. V.; Biniwale, R. B.; Labhsetwar, N. K.; Devotta, S.; Rayalu, S. S. *Energy Fuels* **2007**, *21*, 3555–3559.
(8) Siriwardane, R. V.; Shen, M. S.; Fisher, E. P.; Losch, J. *Energy Fuels* **2001**, *15*, 279–284.
(9) Prezepiórski, J.; Skrodzewicz, M.; Morawski, A. W. *Appl. Surf. Sci.* **2004**, *225*, 235–242.
(10) Lu, C.; Bai, H.; Wu, B.; Su, F.; Hwang, J. F. *Energy Fuels* **2008**, *22*, 3050–3056.
(11) Bae, J. S.; Bhatia, S. K. *Energy Fuels* **2006**, *20*, 2599–2607.
(12) Zhao, X. X.; Xu, X. L.; Sun, L. B.; Zhang, L. L.; Liu, X. Q. *Energy Fuels* **2009**, *23*, 1534–1538.
(13) Zhang, Z. J.; Xu, M. Y.; Wang, H. H.; Li, Z. *Chem. Eng. J.* **2010**, *160*, 571–577.

that can be manipulated by modifying the metal group or organic linker.[14,15] Liu and Smit[16] performed a systematic molecular simulation study to simulate both adsorption selectivity and pure CO_2 and CH_4 adsorption isotherms and determined that MOFs performed much better for CO_2 storage and that their separation performance was comparable to zeolites. Zhao et al.[17] investigated experimentally adsorption equilibria and diffusion of CO_2 on microporous MOF (MOF-5 or IRMOF-1) crystals and reported that the adsorption capacity of CO_2 on MOF-5 was 2.10 mmol/g at 1.0 bar and 296 K, which was much higher than those of conventional adsorbents, such zeolites and activated carbons, and the diffusion coefficient of CO_2 in the MOF-5 was within the range of $8.1-11.5 \times 10^{-9}$ cm^2/s in 295−331 K, with an activation energy of 7.61 kJ/mol. Millward and Yaghi[18] studied the CO_2 uptake over various types of IRMOFs and that MOF-177 was identified to be the best adsorbent for CO_2 at elevated pressures and ambient temperature. However, the framework structures of MOF-5 and MOF-177 were not stable upon H_2O adsorption. The framework structure of MOF-177 was decomposed after its exposure to ambient air in 3 days.[19] Similarly, it was observed that, after MOF-5 was exposed to air for several weeks, the moisture was adsorbed on MOF-5 and, thus, caused decomposition of the structure of MOF-5.[20] The structure stability of MOFs upon water adsorption is an important issue for potential applications of MOFs for gas adsorption and storage materials because H_2O is very difficult to fully remove from industrial gas resources. Li and Yang[19] studied the stability of MOF-177 and MIL-101, and their experimental result showed that MIL-101 could be a promising material for gas adsorption because of its large surface area and pore volume and stability upon H_2O adsorption. Küsgens et al.[21] investigated the water adsorption behavior on some MOFs and found that MIL-101 and ZIF-8 had strong stability upon water adsorption.

MIL-101 (an acronym for Matérial Institute Lavoisier), one of the most porous materials to date,[22−24] has been a very prominent example among the many MOFs. Férey et al.[22] first synthesized and reported its storage capacity of CO_2, which was up to 33 mmol/g CO_2 at 50 bar of pressure. Chowdhury et al.[25] reported the adsorption isotherms of CO_2 on MIL-101 at three different temperatures of 283, 319, and 351 K, and the CO_2 adsorption capacity of MIL-101 at about 5 bar was found to be better than those on silicalite. Hong et al.[26] examined and explained the site-selective functionalization of MIL-101 and demonstrated that the surface amine-grafting undoubtedly provided a general way of selective functionalization of porous MOFs besides that with unsaturated metal sites. However, the kinetic study of CO_2 adsorption on MIL-101 was rarely reported. Both adsorption equilibrium and kinetics are important parameters to evaluate the adsorption performance of an adsorbent. Therefore, it is worthwhile to study the adsorption kinetics of CO_2 on the MIL-101 adsorbent.

The objective of this work is to study the CO_2 adsorption performance on the MIL-101 sample at different temperatures. The MIL-101 crystals would be synthesized, and then the textural properties of the adsorbents were characterized by an accelerated surface area and porosimetry apparatus (ASAP 2010). The isotherms and adsorption kinetic curves of CO_2 on the MIL-101 samples would be separately measured. The isotherms, isosteric adsorption heat, diffusion coefficients, and diffusion activation energies of CO_2 on the MIL-101 samples would be estimated, discussed, and reported here.

2. Experimental Section

2.1. Materials and Instruments. Terephthalic acid (99%+ purity) was purchased from Alfa Chemicals. Chromium nitrate nonahydrate [$Cr(NO_3)_3 \cdot 9H_2O$, 99%, analytical reagent (AR) grade] was purchased from Fuchen Chemicals Co., Ltd. (Tianjin, China). Hydrofluoric acid (AR grade) was purchased from Guangzhou Chemicals Co., Ltd. (Guangzhou, China).

The maganetic suspension balance Rubotherm was from Germany. Its precision was 0.000 001 g. The ASAP 2010 sorptometer was supplied by the Micromeritics Company, Norcross, GA. The microwave-accelerated reaction system Mars-5 was supplied by the CEM Company, Matthews, NC.

2.2. Synthesis and Purification of MIL-101 Crystals. *2.2.1. Synthesis of MIL-101 Crystals.* Synthesis of MIL-101 was performed following the reported procedures,[27] with a few modifications. A total of 2.395 g of chromium nitrate nonahydrate and 0.994 g of benzene dicarboxylate were dissolved in deionized water, and 0.26 mL of hydrofluoric acid was added to the mixture. The reactant mixture was loaded into a Teflon autoclave, sealed, and placed in a microwave oven (Mars-5, CEM). The autoclave was heated to 483 K in 10 min, kept at this temperature for 60 min, and then cooled to room temperature in 3 h. The microwave power was 600 W. A fine green-colored powder was obtained as the major product; significant amounts of H_2bdc were still present in the form of needle-shaped colorless crystals along with the product. To remove this impurity, contents were completely transferred into a conical flask, and *N*,*N*-dimethylformamide was added incrementally with continuous shaking to dissolve H_2bdc. After that, the solution was double-filtrated with glass filters (numbers 1 and 4), followed by the centrifugal process for 30 min at 9000 rad/min. Then, the obtained solids were dried at 423 K, and the MIL-101 crystals were obtained.

2.2.2. Purification of the Synthesized MIL-101 Crystals. As mentioned previously,[24] a significant amount of nonreacted terephthalic acid is present both outside and within the pores of MIL-101, leading to a decrease of its surface area and pore volume. To obtain high porosity, residual terephthalic acid in the as-synthesized MIL-101 crystals in this work can be effectively removed by subsequent solution treatments. A first activation treatment was performed using hot ethanol (95%,

(14) Eddaoudi, M.; Kim, J.; Rosi, N.; Vodak, D.; Wachter, J.; O'Keeffe, M.; Yaghi, O. M. *Science* **2002**, *295*, 469–472.
(15) Karra, J. R.; Walton, K. S. *Langmuir* **2008**, *24*, 8620–8626.
(16) Liu, B.; Smit, B. *Langmuir* **2009**, *25*, 5918–5926.
(17) Zhao, Z. X.; Li, Z.; Lin, Y. S. *Ind. Eng. Chem. Res.* **2009**, *48*, 10015–10020.
(18) Millward, A. R.; Yaghi, O. M. *J. Am. Chem. Soc.* **2005**, *127*, 17998–17999.
(19) Li, Y. W.; Yang, R. T. *AIChE J.* **2008**, *54*, 269–279.
(20) Huang, L. M.; Wang, H. T.; Chen, J. X.; Wang, Z. B.; Sun, J. Y.; Zhao, D. Y.; Yan, Y. S. *Microporous Mesoporous Mater.* **2003**, *58*, 105–114.
(21) Küsgens, P.; Rose, M.; Senkovska, I.; Fröde, H.; Henschel, A.; Siegle, S.; Kaskel, S. *Microporous Mesoporous Mater.* **2009**, *120*, 325–330.
(22) Férey, G.; Mellot-Draznieks, C.; Serre, C.; Millange, F.; Dutour, J.; Surblé, S.; Margiolaki, I. *Science* **2005**, *309*, 2040–2042.
(23) Chen, B. L.; Ockwig., N. W.; Millward, A. R.; Contreras, D. S.; Yaghi, O. M. *Angew. Chem., Int. Ed.* **2005**, *44*, 4745–4749.
(24) Hwang, Y. K.; Hong, D.-Y.; Chang, J.-S.; Jhung, S. H.; Seo, Y.-K.; Kim, J.; Vimont, A.; Daturi, M.; Serre, C.; Férey, G. *Angew. Chem., Int. Ed.* **2008**, *47*, 4144–4148.
(25) Chowdhury, P.; Bikkina, C.; Gumma, S. *J. Phys. Chem. C* **2009**, *113*, 6616–6621.
(26) Hong, D.-Y.; Hwang, Y. K.; Serre, C.; Férey, G.; Chang, J.-S. *Adv. Funct. Mater.* **2009**, *19*, 1537–1552.
(27) Jhung, S. H.; Lee, J. -H.; Yoon, J. W.; Serre, C.; Férey, G.; Chang, J.-S. *Adv. Mater.* **2007**, *19*, 121–124.

v/v) at 373 K for 20 h until no colored impurities were detected in the mother liquor solution. The second activation treatment was performed using an aqueous solution of 30 mmol/L NH_4F at 333 K for 10 h. After cooling, the precipitate was centrifuged and washed 5 times with 200 mL of hot water (333 K) to remove traces of NH_4F. Finally, the synthesized MIL-101 crystals were dried using a vacuum oven at 423 K for 8 h.

2.3. Characterization of MIL-101 Crystals. The MIL-101 sample was characterized for its pore textural properties with nitrogen adsorption and desorption at liquid nitrogen temperature using an accelerated surface area and porosimetry system (ASAP 2010, Micromeritics). The pore textural properties, including specific Langmuir and Brunauer−Emmett−Teller (BET surface areas, pore volume, and pore size, were obtained by analyzing the nitrogen adsorption and desorption isotherms with the Micromeritics ASAP 2010 built-in software. Before the nitrogen adsorption measurements were started, the sample was activated by degassing *in situ* at 423 K for 12 h to remove any guest molecule from the pores of the MIL-101 crystals.

The MIL-101 sample was also investigated for its crystal phase structure by a Bruker D8 Advance X-ray diffractometer with Cu Kα emission and 40 kV/40 mA current. The X-ray scanning speed was set at 2°/min and a step size of 0.02° in 2θ. A jade 5 X-ray diffraction (XRD) pattern processing software (MDI, Inc., Livermore, CA) was used to analyze the XRD data collected on the MIL-101 sample.

Thermal stability of the MIL-101 sample was characterized using a thermogravimetric analyzer (TGA) STA449C, NETZSCH, Germany. About 10 mg of the sample was placed in the TGA, and the temperature was ramped from 298 to 800 K at 2 K/min in continuous N_2 flow (30 cm^3/min).

The surface morphology and particle size of the crystalline MIL-101 sample were observed by a S4800 scanning electron microscope at an accelerating voltage of 40 kV after gold deposition on the sample surface.

2.4. CO_2 Adsorption Study. *2.4.1. Determination of Adsorption Isotherms of CO_2 on MIL-101.* In this work, the CO_2 adsorption−desorption isotherms at 298, 308, 318, and 328 K were obtained on a Rubotherm magnetic suspension balance. This balance is equipped with an automatic flow gas dosing and pressure control system, and it can be used to measure both adsorption−desorption equilibrium automatically at temperatures ranging from 223 to 723 K. At first, 0.2 g of the adsorbent was introduced into the sample container, which was placed on the magnetic suspension balance located in the measuring cell. Then, the initial activation of the MIL-101 sample was carried out at 423 K for 12 h in a vacuum environment before the adsorption experiment started; i.e., the weight of the sample MIL-101 would be periodically recorded with the help of the magnetic suspension balance as the adsorption occurred. He (ultra-high purity, U-sung) was used as a purge gas in this study. The adsorption processes were carried out using high-purity CO_2 (99.999%) gas. After that, feed flow rates of 60 mL/min CO_2 and 30 mL/min He were controlled with the mass flow controllers (MFCs) to the sample chamber. Both adsorption and desorption experiments were conducted at the same temperature. The temperature of the sorption chamber could be adjusted and maintained constant by an internal temperature sensor. The pressure could be regulated via a back-pressure controller. The operation was run in dynamic mode.

The recorded balance reading (m_{BAL}) in the adsorption measurement needed to be corrected for the buoyancy effect acting on the sample and sample container. This was performed by adding the product of the density of the gas (ρ) and the volume of the sample and sample container (V_{SC+S}, determined in the buoyancy measurement before) to the balance reading

$$m_{BAL,CORR} = m_{BAL} + \rho V_{SC+S} \quad (1)$$

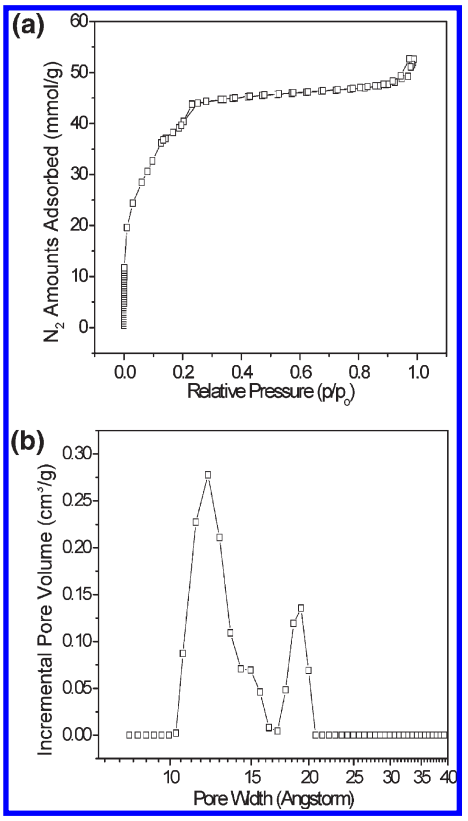

Figure 1. (a) Adsorption−desorption isotherm of N_2 on MIL-101. (b) DFT pore size distribution of MIL-101.

Then, the mass of the sample with adsorbed gas (m) was determined by

$$m = m_{BAL,CORR} - m_{SC} \quad (2)$$

where V_{SC+S} is the volume of the loaded sample container, calculated from the buoyancy measurement. ρ can be calculated using an appropriate thermal equation of state.

2.4.2. Determination of Adsorption Kinetic Curves of CO_2 on MIL-101. The CO_2 adsorption kinetic experiments at 0.5, 3.0, and 20.0 bar with different temperatures were obtained on the Rubotherm magnetic suspension balance. First, the MIL-101 sample was degassed at 423 K for 12 h in a vacuum environment before the adsorption experiment started. Then, the adsorption kinetic curves giving the amounts adsorbed of CO_2 on the MIL-101 sample as a function of time were measured. Second, a feed flow rate of 60 mL/min of CO_2 was controlled with the MFC to the sample chamber. Finally, the adsorption kinetic experiment ended when the weight of the sample became unvaried, meaning that the equilibrium had been achieved (the sample was saturated with CO_2).

3. Results and Discussion

3.1. Physical Properties of MIL-101. *3.1.1. Pore Texture Properties.* Figure 1a shows the nitrogen adsorption−desorption isotherm of the MIL-101 sample. The N_2 isotherm on the MIL-101 sample is of a type-I isotherm, with an initial steep increase in the nitrogen uptake followed by a plateau. In addition, it is found that there are secondary uptakes at $p/p_0 = \sim 0.1$ and ~ 0.2, characterizing the presence of two kinds of microporous windows (pentagonal and hexagonal windows).[22] Figure 1b gives the pore size distribution profile of the synthesized MIL-101, calculated using the density functional theory (DFT). The plot shows the existence of two maxima centered at a pore radius of ca. 12.1

Table 1. Texture Properties of MIL-101 and a Comparison of Their Properties to Those Reported in the Literature

samples	surface area (cm^2/g)	pore volume (cm^3/g)	synthesized methods	reference
MIL-101	3360	1.75	microwave assisted	current study
MIL-101	2674	1.38	hot air oven	19
MIL-101	3900	2.3	microwave assisted	25
MIL-101	3780	1.74	microwave assisted	26
MIL-101	4230	2.15	microwave assisted	26
MIL-101	2931	1.45	conventional hydrothermal	27
MIL-101	3200	2.1	conventional hydrothermal	28
MIL-101	2693	1.30	conventional hydrothermal	29

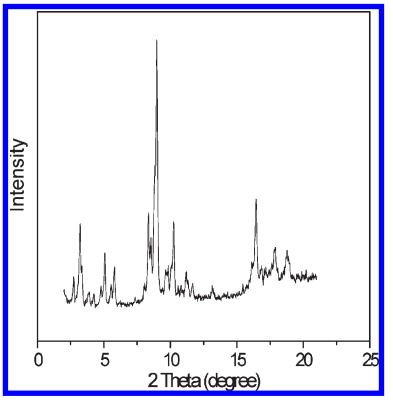

Figure 2. Powder XRD pattern of synthesized MIL-101.

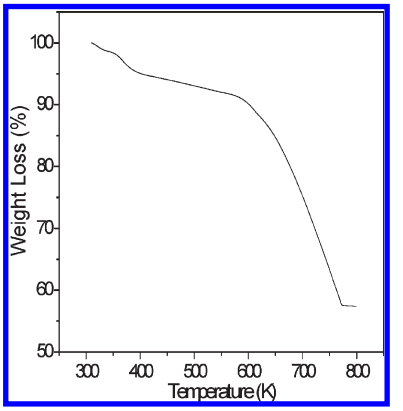

Figure 3. Thermogravimetric analysis of synthesized MIL-101.

and 19.2 Å. In addition, the MIL-101 sample prepared in this work has ideal pore textural properties with large Langmuir (4792 m^2/g) and BET (3360 m^2/g) specific surface areas and a large total pore volume of 1.75 cm^3/g. Table 1 gives the physical characteristics of MIL-101 used in other works in the literature. It can be seen that there are slight variations between the surface area and pore volume results obtained in this work and those in other works in the literature, which may be attributed to the presence of varying degrees of terephthalic acid formed during microwave irradiation. Llewellyn et al.[30] indicated that the post-treatment procedures in the synthesis of MIL-101 had a significant influence on the structure parameters of synthesized MIL-101 and, thus, its adsorption properties.

3.1.2. XRD Pattern of the MIL-101 Sample. Figure 2 shows the powder X-ray diffraction (PXRD) of the synthesized MIL-101 sample. The main peaks in the XRD pattern of the MIL-101 sample match well with the published XRD pattern for MIL-101.[19,27]

3.1.3. Thermogravimetric Analysis of MIL-101. Figure 3 shows the thermogravimetric analysis of the MIL-101 sample. It shows two distinct weight loss steps. The first step, in the range from 298 to 573 K, corresponds to the loss of guest water molecules, and the second weight loss step (600−770 K) is due to the elimination of OH/F groups, leading to the decomposition of the frameworks.[22]

3.1.4. Scanning Electron Microscopy (SEM) Analysis of MIL-101. Figure 4 shows the SEM image of the MIL-101 sample prepared in this work. It can be seen that the crystals

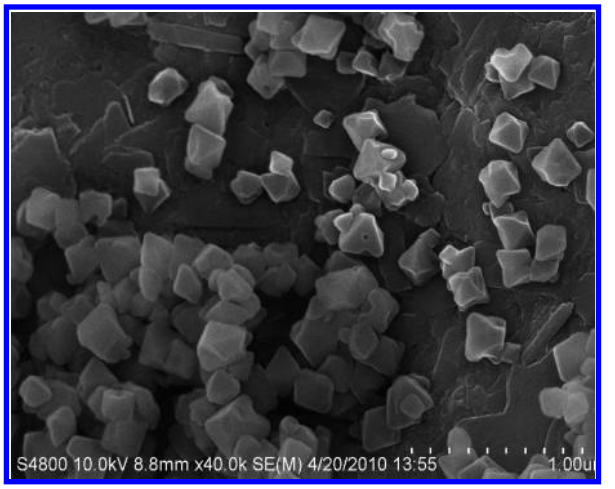

Figure 4. SEM image of the MIL-101 octahedron crystals prepared in this work.

are of octahedron shape, with sizes in the range of 40−160 nm, which are much lower than those reported in the recent literature using conventional hydrothermal synthesis techniques.[25] Jhung et al.[27] also found that the MIL-101 crystals synthesized using microwave irradiation methods are smaller than those synthesized with conventional hydrothermal methods.

3.2. Isotherms of CO_2 on MIL-101 Crystals. Figure 5 shows adsorption isotherm data of CO_2 on MIL-101 at different temperatures measured experimentally and Freundlich isotherms, which are typically represented as $q = kp^{1/n}$. Table 2 lists the values of Freundlich isotherm fitting parameters and the regression coefficients. It can be seen that the experimental isotherm data are in fair agreement with Freundlich model predictions, and the correlation coefficients

(28) Maksimchuk, N. V.; Timofeeva, M. N.; Melgunov, M. S.; Shmakov, A. N.; Chesalov, Y. A.; Dybtsevb, D. N.; Fedinb, V. P.; Kholdeeva, O. A. *J. Catal.* **2008**, *257*, 315–323.
(29) Liu, Y. Y.; Zeng, J. L.; Zhang, J.; Xu, F.; Sun, L. X. *Int. J. Hydrogen Energy* **2007**, *32*, 4005–4010.
(30) Llewellyn, P. L.; Bourrelly, S.; Serre, C.; Vimont, A.; Daturi, M.; Hamon, L.; Weireld, G. D.; Chang, J.-S.; Hong, D.-Y.; Hwang, Y. K.; Jhung, S. H.; Férey, G. *Langmuir* **2008**, *24*, 7245–7250.

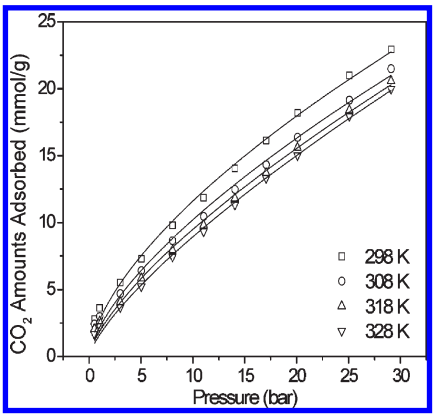

Figure 5. Comparison between the measured and Freundlich model profiles for CO_2 adsorption on MIL-101 at various temperatures.

Table 2. Freundlich Isotherms for CO_2 Adsorption on MIL-101

	Freundlich		
temperature (K)	K_F (g^{-1})	n	R^2
298	0.153	1.87	0.993
308	0.129	1.80	0.991
318	0.112	1.70	0.991
328	0.094	1.58	0.993

$R \geq 0.99$ are available. The data in Table 2 indicate that the values of K_F gradually decrease with the temperature, consistent with the physisorption behavior,[32] and the adsorption intensity n larger than unity confirms that the adsorption of CO_2 on MIL-101 is favorable under studied conditions. These findings infer that the Freundlich isotherm equation fits the experimental data well. In addition, the experimental isotherm data show a modest increase in the amount adsorbed of CO_2 with the increase of the pressure. Furthermore, it is noticed that there are no plateaus in adsorption isotherms in the pressure range investigated, indicating that MIL-101 can adsorb more CO_2 with the increase of CO_2 pressures. As shown in Figure 5, the maximum adsorption capacity of CO_2 on MIL-101 is found at 22.9 mmol/g at 298 K and 30 bar. This corresponds to a percentage of monolayer coverage of 25.9% under studied conditions, which can be found out according to the following equation:

$$X_{\text{monolayer}} = qA_0N_A/S_A$$

where q (mmol/g) is the uptake capacity, S_A is the Langmuir surface area (4792 m^2/g), A_0 is the adsorbate cross-sectional area estimated from the molecular kinetic diameter assuming a spherical shape (9 $Å^2$ for CO_2[31]), and N_A is Avogadro's number (6.02×10^{23} molecule/mol).

For comparison, parts a and b of Table 3 list the adsorption capacities of some adsorbents at low and high pressures reported by some other investigators and available in the present work for CO_2 adsorption. The data in parts a and b of Table 3 indicate that MIL-101 synthesized in this work has a higher adsorption capacity of CO_2 than some conventional adsorbents, such as zeolite 13X, activated carbon, and some new MOFs. However, it should be mentioned that, at higher pressure, the adsorption capacity of MIL-101 for CO_2 is lower than that of MOF-177, as shown in Table 3b, but at low pressure, the adsorption capacity of MIL-101 for CO_2 is almost 5 times that of MOF-177, as indicated in Table 3a. It indicates that MIL-101 is suitable to capture CO_2 at low pressure.

3.3. Isosteric Heat of Adsorption. Isosteric heat (enthalpy) of adsorption is also an important criterion, characterizing the interaction between the adsorbate molecules and the adsorbent surfaces. The isosteric heats of adsorption as a function of the surface coverage are calculated from isotherms at different temperatures using the following van't Hoff's equation:

$$\frac{\Delta H_S}{RT^2} = -\left(\frac{\partial \ln p}{\partial T}\right)_q \quad (3)$$

where ΔH is the isosteric heat of adsorption at specific loading (kJ/mol), T is the temperature, p is the pressure (bar), q is the amount adsorbed (mmol/g), and R is the universal gas constant. Integrating eq 3 gives

$$\ln p = \frac{\Delta H_S}{RT} + C \quad (4)$$

where C is an integration constant.

The isotherms of CO_2 at 298, 308, 318, and 328 K were used to calculate the heat of adsorption. First, the CO_2 adsorption isotherms were converted to CO_2 adsorption isosteres, a plot of p versus T at a given adsorption amount. Then, the adsorption heats of CO_2 were found out from the slopes of isosteres according to eq 4. The adsorption heats of CO_2 in MIL-101 are about 4.0−28.6 kJ/mol, as shown in Figure 6. It can be observed that the isosteric heat of adsorption varies with the surface loading, indicating that MIL-101 has an energetically heterogeneous surface for CO_2 adsorption. This is because the isosteric heat of adsorption at low coverage is related to the sorbate−sorbent interaction potential.[38] At low coverage, there exists a strong interaction between the CO_2 molecules and the unsaturated Cr^{III} metal sites, while at a higher coverage, the interactions between the CO_2 molecule and the pentagonal and hexagonal windows become a little lower.[25] Other researchers have also reported the isosteric heats of CO_2 adsorption on some other adsorbents. Zhao et al.[17] studied the adsorption behavior of CO_2 on MOF-5 and reported that the adsorption heat was 34.1 kJ/mol. Hyun et al.[39] calculated the isosteric heat of CO_2 adsorption on zeolite 13X and found that it was 33−34 kJ/mol. The relatively low value of isosteric heat of CO_2 adsorption on MIL-101 indicates that CO_2 has a moderate interaction with the framework of MIL-101, as compared to MOF-5 and zeolite 13X.

3.4. CO_2 Adsorption Kinetics. To evaluate the adsorption rate of CO_2 on the MIL-101 crystals, it is necessary to determine their mass-transfer coefficients. Suppose M g of

(31) Guo, B.; Chang, L. P.; Xie, K. C. *J. Nat. Gas. Chem.* **2006**, *15*, 223–229.
(32) Saha, D.; Wei, Z. J.; Deng, S. G. *Sep. Purif. Technol.* **2009**, *64*, 280–287.
(33) Shen, C. Z.; Grande, C. A.; Li, P.; Yu, J. G.; Rodrigues, A. E. *Chem. Eng. J.* **2010**, *160*, 398–407.
(34) Walton, K. S.; Millward, R. A.; Dubbeldam, D.; Frost, H.; Low, J. J.; Yaghi, O. M.; Snurr, R. Q. *J. Am. Chem. Soc.* **2008**, *130*, 406–407.
(35) Furukawa, H.; Yaghi, O. M. *J. Am. Chem. Soc.* **2009**, *131*, 8875–8883.
(36) Kitagawa, S.; Kitaura, R.; Noro, S. *Angew. Chem., Int. Ed.* **2004**, *43*, 2334–2375.
(37) Llewellyn, P. L.; Bourrelly, S.; Serre, C.; Filinchuk, Y.; Férey, G. *Angew. Chem., Int. Ed.* **2006**, *45*, 7751–7754.
(38) Yang, R. T. *Adsorbents: Fundamentals and Applications*; Wiley-Interscience: New York, 2003.
(39) Hyun, S. H.; Danner, R. P. J. *Chem. Eng. Data* **1982**, *27*, 196–200.

Table 3. Comparison of the Adsorption Capacity of MIL-101 to Those of (a) Some Other Adsorbents and (b) Various Adsorbents at Higher Pressure

adsorbent	adsorption capacity (mmol/g)	pressure (bar)	temperature (K)	reference
(a) Comparison of the Adsorption Capacity of MIL-101 to Those of Some Other Adsorbents				
MIL-101 (microwave)	3.62	1.0	298	current study
zeolite 13X	2.2	1.0	298	1
$AlPO_4$-14	2.00	1.0	300	12
AC	2.92	1.0	298	13
AAC	3.22	1.0	298	13
HAC	3.49	1.0	298	13
MOF-5	2.10	1.0	296	17
Norit RB2	2.50	1.0	298	18
IRMOF-1 (hydrothermal)	1.92	1.0	208	18
IRMOF-11	1.8	1.1	298	18
MOF-505	3.30	1.0	298	23
activated carbon beads	1.92	1.0	303	33
MOF-177	0.8	1.0	298	34
COF-6	3.61	1.0	273	35
(b) Comparison of the Adsorption Capacity of MIL-101 to Those of Various Adsorbents at Higher Pressure				
MIL-101	22.9	30	298	current study
IRMOF-1	21.3	30	298	34
IRMOF-3	18.6	32	298	34
MOF-177	32.8	31	298	34
COF-6	12.1	30	298	35
activated carbon Norit R1	10	30	298	36
IRMOF-1	21.7	35	298	37

adsorbent was suddenly placed in CO_2 flow. At time $t > 0$, adsorption of CO_2 occurred, and the amount adsorbed, $q(t)$, of CO_2 on the adsorbent increased with time. The adsorption rate of CO_2 was assumed to follow first-order kinetics [linear driving force (LDF) model], with the following equation used to describe the adsorption process:[40,41]

$$\frac{\partial \overline{q}}{\partial t} = k_{\text{eff}}(q^* - q) \tag{5}$$

where k_{eff} is the mass-transfer constant, q^* is the equilibrium amount adsorbed of CO_2 corresponding to the CO_2 concentration of the gas phase at some temperature, and $q(t)$ is the CO_2 amount taken by the adsorbent at time t, which can be found using a gravimetric measurement method. From eq 5, the integral equation was available as follows:

$$\ln\left(\frac{q^* - q}{q^*}\right) = -k_{\text{eff}}t \tag{6}$$

If an adsorption experiment of CO_2 is conducted at a certain pressure, the corresponding kinetic curve, $q(t)-t$ curve, could be obtained. After that, a plot of $-\ln(q^* - q)/q^*$ versus t will yield a line with slope k_{eff}. As a result, from the slope of the line, k_{eff} can be found.

Panels a−c of Figure 7 show the kinetic curves of CO_2 adsorption on MIL-101. On the basis of the kinetic curves, the mass-transfer constants of CO_2 can be found according to eq 6. Figure 7d shows the plots of $\ln(q^* - q)/q^*$ versus time for CO_2 adsorption on MIL-101. The plots were linearly fitted, with correlation coefficients (R^2) more than 0.99, indicating that the adsorption process of CO_2 can be well-described by eq 6. From the slopes of these lines, the mass-transfer constants of CO_2 were obtained, as listed in Table 4.

The data in Table 4 indicated that the mass-transfer coefficients increased with the temperature because the diffusion of the CO_2 molecule became quicker with the temperature and decreased with the increase of the pressure because molecular diffusion resistance became larger with the pressure.

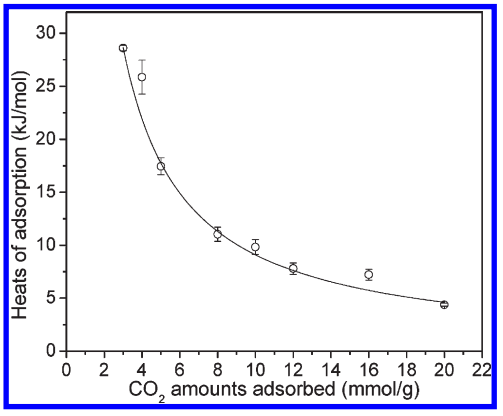

Figure 6. Effect of the adsorption amount on the isosteric heat of adsorption of CO_2 on MIL-101.

In addition, the diffusion coefficient, D_e, of CO_2 within MIL-101 can be estimated on the basis of the mass-transfer coefficients of CO_2 listed in Table 4. Interparticle diffusion is supposed to be the rate-limiting step, and thus, a diffusion coefficient, D_e, can be calculated using eq 7[42]

$$D_e = \frac{k_{\text{eff}} {R_p}^2}{15} \tag{7}$$

where D_e (cm^2/s) is the intracrystalline diffusion coefficient, R_p (cm) is the crystal radius (2×10^{-3} cm), and k_{eff} (s^{-1}) is the mass-transfer coefficient.

Table 4 lists the diffusion coefficients, D_e, of CO_2 within MIL-101 and their standard deviations (SDs). The diffusion coefficients (D_e) are in the range from 4.11×10^{-11} to 2.54×10^{-10} cm^2/s. The coefficients increase with the temperature and decrease with the pressure.

(40) Kennedy, L. J.; Vijaya, J. J.; Sekaran, G.; Kayalvizhi, K. *J. Hazard. Mater*. **2007**, *149*, 134–143.
(41) Li, Z.; Yang, R. T. *AIChE J*. **1999**, *45*, 196–200.
(42) Roque-Malherbe, R. M. A. *Adsorption and Diffusion in Nanoporous Materials*; CRC Press: Boca Raton, FL, 2007.

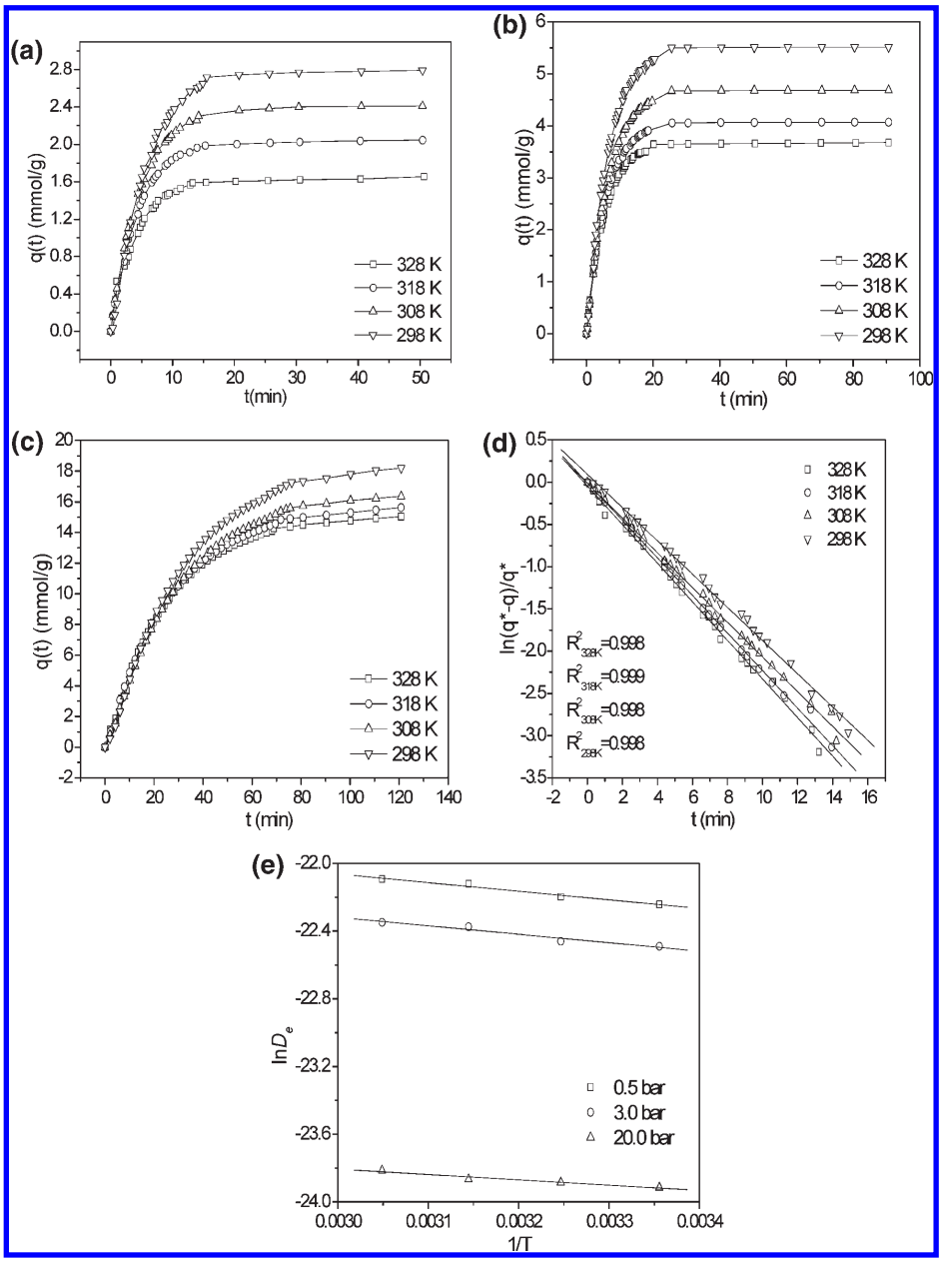

Figure 7. (a) Adsorption kinetics curves of CO_2 on the MIL-101 crystals at (a) 0.5 bar, (b) 3.0 bar, and (c) 20.0 bar with different temperatures. (d) Linear dependence between $\ln(1 - q/q^*)$ and time for the analysis of CO_2 adsorption kinetics on the MIL-101 crystal using the LDF model at 0.5 bar with different temperatures. (e) Linear dependence between $\ln D_e$ and $1/T$ for the estimation of CO_2 diffusion activation energies on the MIL-101 crystals.

Table 4. Kinetics Parameters and Diffusion Activation Energy of CO_2 on MIL-101[a]

parameters	temperatures (K)	at 0.5 bar	$SD_{0.5\ bar}$[b] (±)	at 3.0 bar	$SD_{3.0\ bar}$[b] (±)	at 20.0 bar	$SD_{20.0\ bar}$[b] (±)
mass-transfer coefficients k_{eff} ($\times 10^{-4}$ s^{-1})	298	32.8	0.0184	25.7	0.0152	6.17	0.00494
	308	34.3	0.0176	26.4	0.00745	6.36	0.00458
	318	37.1	0.0149	28.8	0.00931	6.48	0.00294
	328	38.1	0.0211	29.6	0.0113	6.82	0.00473
diffusion coefficients D_e ($\times 10^{-11}$ cm^2/s)	298	21.9	0.0184	17.1	0.0152	4.11	0.00494
	308	22.9	0.0176	17.6	0.00745	4.24	0.00458
	318	24.7	0.0149	19.2	0.00931	4.32	0.00294
	328	25.4	0.0211	19.7	0.0113	4.55	0.00473
diffusion activation energy, E_a (kJ/mol)		4.24	0.182	4.16	0.265	2.62	0.159

[a] The average particle radius, R_p, of the MIL-101 crystal is 10 μm. [b] SD = standard deviation.

After a series of the diffusion coefficients, D_e, of CO_2 at different temperatures were available, the diffusion activation energy of CO_2 can be estimated by means of the Arrhenius equation

$$D_e = A \exp(-E_a/RT) \quad (8)$$

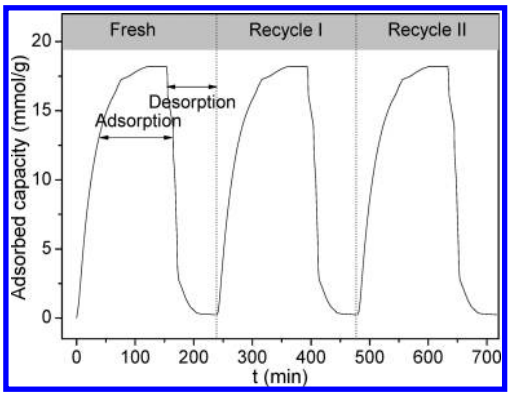

Figure 8. Recycle runs of CO_2 adsorption on MIL-101.

where E_a, A, and R refer to the Arrhenius activation energy, Arrhenius factor, and gas constant, respectively. Equation 8 can also be expressed as

$$\ln D_e = \ln A - E_a/RT \quad (9)$$

When $\ln D_e$ is plotted to $(1/T)$ according to the data in Table 4, a straight line [slope $= -(E_a/R)$] can be obtained. Thus, the diffusion activation energy E_a can be directly calculated from the slope of the straight line.

Figure 7e shows the plots of $\ln D_e$ versus the inverse temperature $(1/T)$ in an Arrhenius-type plot. The plots were linearly fitted, with correlation coefficients (R^2) more than 0.95, showing a good linearity between $\ln D_e$ and $1/T$. Thus, the diffusion activation energies E_a of CO_2 on MIL-101 were available from the slope of the straight line, which was in the range of 2.62−4.24 kJ/mol, as shown in Table 4. Zhao et al.[17] studied the adsorption and diffusion of CO_2 on the MOF-5 cubes and reported that the diffusion activation energy of CO_2 was 7.61 kJ/mol. In other words, the diffusion activation energy, E_a, of CO_2 on MIL-101 is lower than that of CO_2 on the MOF-5 sample, meaning that the diffusion rate of CO_2 within MIL-101 is higher than that within MOF-5. Moreover, the data in Table 4 also indicate that E_a of CO_2 decreased with the pressure, suggesting that the adsorption of CO_2 was easier at higher pressures.

Finally, Figure 8 shows the performance of MIL-101 in three consecutive CO_2 adsorption−desorption runs within 750 min at 298 K and 20 bar. No detectable deterioration in adsorption capacity was observed, confirming the reproducibility and stability of the material.

4. Conclusions

CO_2 adsorption equilibrium and kinetics were studied gravimetrically on MOF (MIL-101) crystals synthesized in this study. The MIL-101 sample synthesized by microwave irradiation in this work was of octahedron crystals of 40−160 nm in size, with a Langmuir surface area of 4792 m^2/g. The isotherms of CO_2 on MIL-101 can be well-fitted with the Freundlich isotherm equation, and the adsorption kinetics of CO_2 can be well-described by the LDF model. The maximum uptake amount of CO_2 on MIL-101 is 22.9 mmol/g at 298 K and 30 bar. The isosteric adsorption heat of CO_2 in MIL-101 is in the range of 4.0−28.6 kJ/mol. The heat of adsorption depends upon the amount of CO_2 uptake and decreases with the amount adsorbed of CO_2. The diffusion coefficients of CO_2 are in the range from 4.11×10^{-11} to 2.54×10^{-10} cm^2/s. The coefficients increase with the temperature and decrease with the pressure. The diffusion activation energies, E_a, of CO_2 on MIL-101 are in the range of 2.62−4.24 kJ/mol, which decreased with the pressure.

Acknowledgment. The authors thank the National Natural Science Foundation of China (Grant 20936001), the Science and Technology Foundation of Guangdong Province, and the State Key Lab of Subtropical Building Science, South China University of Technology (Grant 2010ZC19) for financial support.